Supporting information

Text S1 Experimental details of potentiometric titration

All titrations were conducted in a 100 mL beaker at 298K. Prior to titration, 50 mg samples were suspended in 0.1 mol/L $NaNO_3$ solution (50 mL) and purged with N_2 gas for 1 h. The solution pH was first titrated to 3.0 using HNO_3 solution (0.2 mol/L). After that, the suspension was slowly back-titrated using NaOH solution (0.030 mol/L) until pH reached 11. Each step was allowed to stabilize until the pH drift was less than 0.005 per minute. All solutions were prepared with pre-boiled deionized water and then kept under a nitrogen atmosphere. Moreover, high-purity N_2 gas was bubbled into solutions throughout the experiments.

The net surface charge Q_H (mmol/g-Zr) was calculated as (Eq. (S1)):

$$Q_H = \frac{(V_{A(T)}C_A - V_B C_B)/V_T + [H^+] - [OH^-]}{m} V_T \quad (S1)$$

where $V_{A(T)}$ (mL) is the total volume of the HNO_3 added; V_B (mL) is volume of the titrated NaOH; C_A and C_B (mol/L) are the molar concentrations of the HNO_3 and NaOH added, respectively; $[H^+]$ and $[OH^-]$ (mol/L) are the activities of the aqueous H^+ and OH^- in the solutions; V_T (L) is the solution volume; and m (g) is mass of the sample titrated (in terms of the mass of Fe).

FITEQL 3.1 software (Armando Herbelin and John C. Westall, Oregon State University, USA) was applied to simulate surface acid-base properties onto the HZO@N201/ZrP@N201. A 2-pK method was applied to simulate potentiometric titration data in order to evaluate surface acid-base properties (Lützenkirchen, 1998). More detail seen in Table S2.

Text S2 The mathematical derivation process of the mass flow rate equation

The mass flow rate of fluoride is given by the expression of Eq (S2):

$$-\frac{dC}{dt} = k_f \cdot a(C - C_s) \quad (S2)$$

where k_f is the mass transfer coefficient (cm/s), a is the specific area available for mass transfer per unit volume of the contactor (m^2/m^3), C is the concentration of fluoride in bulk solution

(mol/L), C_s is the concentration of fluoride at interface (mol/L). Assume the adsorption fit linear isotherm Eq (S3):

$$q = \frac{q_m k C_s}{1 + k C_s} \qquad \text{(S3)}$$

where k is the adsorption equilibrium coefficient (L/mmol) and q is the adsorption capacity (mg/g), which can be calculated by the following Eq (S4):

$$q = \frac{V}{m}(C_0 - C_s) \qquad \text{(S4)}$$

where V is the contactor volume (0.5 L), m is the mass of nanocomposite (0.25 g), and C_0 is the initial concentration of fluoride in bulk solution (10 mg/L). Combining Eqs. (S2)–(S4) yields Eq (S5):

$$-\frac{dC}{dt} = k_f a\left[C - \frac{1}{2}\left(\sqrt{\left(\frac{q_m m}{V} - C_0 + \frac{1}{k}\right)^2 + \frac{4C_0}{k}} - \frac{q_m m}{V} + C_0 - \frac{1}{k}\right)\right] \qquad \text{(S5)}$$

To describe the sorption data with the model, we derived the concentration of fluoride in bulk solution (C) as a function of time (t) with Eq. (S6):

$$C = b\exp[-ht] + C_0 - b \quad , \qquad \text{(S6)}$$

In Eq. (S6), h and b are the fitting parameters. $h = k_f a$ and $b = C_0 - \frac{1}{2}\left(\sqrt{\left(\frac{q_m m}{V} - C_0 + \frac{1}{k}\right)^2 + \frac{4C_0}{k}} - \frac{q_m m}{V} + C_0 - \frac{1}{k}\right)$. Combining Eqs. (S4) and (S6) yields Eq. (S7):

$$q = \frac{b(1-\exp[-ht])}{m} V \quad , \qquad \text{(S7)}$$

Thus Eq. (S7) is used to fit the experimental results with h and b as fitting parameters.

Text S3 Fitting of adsorption isotherms

The adsorption isotherms of HZO@N201and ZrP@D201 conform well to the Langmuir model (Eq. (S8)):

$$Q_e = \frac{Q_m K_L C_e}{1 + K_L C_e} \quad , \qquad \text{(S8)}$$

where Q_e is the equilibrium adsorption capacity of fluoride (mg/g); C_e is the equilibrium concentration of fluoride in solution (mg/L); Q_m is the maximum fluoride adsorption (mg/g); and K_L is the Langmuir adsorption isotherm coefficient. The K_L value can roughly reflect the adsorption affinity toward target pollutants.

Text S4 DFT calculation of fluoride adsorption by the nano-adsorbents

The first-principles-based simulations were performed using CP2K code (Kresse and Joubert, 1999). For the MD calculations, the NVT ensemble was used. The GFN-xTB tight binding method is employed in this study. The "melt-and-quench" approach was used to obtain the amorphous structure of materials. The temperature is controlled with a Nose − Hoover thermostat attached to every degree of freedom to ensure equilibration and the integration time step was 1.0 fs. The atoms in the cells were melted at 400K for 2000 MD steps and quenched from 400K to 300K for 2000 MD steps. The surface slab was constructured with obtained amorphous materials of ZrO and ZrPOH. The Vienna ab initio Simulation Package (VASP) was used to calculate the energy of the adsorption systems under the framework of density functional theory (Ataka et al., 1996). The generalized gradient approximation (GGA) with the Perdew-Burke-Ernzerhof (PBE) function was used for the evaluation of the exchange-correlation energy (Martínez et al., 2009). The plane-wave basis set was set to an energy cutoff of 400 eV to provide accurate self-consistent charge density. The atomic force convergence criterion of 0.001 eV Å-1 was used to identify optimized geometries. The model of the surface slab was constructed with an ample vacuum space of 15 Å. The Brillouin zone was sampled with 1 × 2 × 1 gamma grid for geometry optimizations. The DFT-D3 dispersion correction method was used to describe the weak interaction between adsorbent and adsorbate. The adsorption energy of the system (E_{ads}) was calculated by Eq. (S9):

$$E_{ads} = E_{sub/F} - E_{sub} - E_F \quad , \quad (S9)$$

where $E_{Sub/F}$ is the total energy of amorphous ZrO or ZrPOH adsorption of F ion, E_{sub} is the energy of amorphous ZrO or ZrPOH, E_F is the energy of the adsorbate (Perdew et al., 1996; O'Connor et al., 2018).

Table S1 The basic properties of the N201 hosts.

Material	Appearance	Color	Skeleton	Functional group	BET surface area (m^2/g)	Pore volume (cm^3/g)	Average pore diameter (nm)
N201	Spherical beads, ~0.8 mm in diameter	Transparent	Poly (styrene-co-divinylbenzene)	$-N^+(CH_3)_3$	5.9	0.013	4.9

Table S2 The result of the simulate potentiometric titration data.

No.	Components	≡ZrOH	≡POH	H^+	PSI	log K
1	H^+	0	0	1	0	0
2	OH^-	0	0	–1	0	−13.997
3	≡ZrOH	1	0	0	0	0
4	$≡ZrOH_2^+$	1	0	1	1	12.300
5	≡POH	0	1	0	0	0
6	$≡PO^-$	0	1	−1	−1	−10.000

From potentiometric titration data, the total proton concentration TOTH (mmol/L) was calculated and simulated with SCMs to obtain log K.

Table S3 The results of the mass transfer model fitting.

Adsorbent	h (s^{-1})	a (m^2/m^3)	k_f (cm/s)	b (mg/L)
ZrP@N201	7.7×10^{-4}	21597	3.56×10^{-6}	22.08
HZO@N201	1.7×10^{-4}	37350	4.55×10^{-7}	13.14
ZrP bulks	7.3×10^{-4}	16129	4.53×10^{-6}	5.26

Table S4 The results of split-peak fitting of Zr 3d XPS analysis.

Adsorbent	state	Bingind energy of Zr in Zr-O (eV)		Bingind energy of Zr in Zr-F (eV)		Peak area ratio
		$3d_{5/2}$	$3d_{3/2}$	$3d_{5/2}$	$3d_{3/2}$	
ZrP@N201	Before adsorption	182.7	185.1	—	—	3:2
	After adsorption	182.7	185.1	184.3	186.7	3:2:3.57:2.38
HZO@N201	Before adsorption	183.3	185.7	—	—	3:2
	After adsorption	183.3	185.7	184.3	186.7	3:2:2.66:1.78

Table S5 The base parameters of the simulated groundwater and the real wastewater.

Project	Unit	Simulated groundwater	Industrial wastewater
pH	—	7.0/5.0	6.7
TOC	mg-C/L	0	6.25
fluoride	mg/L	3.8/3.7	3.6
silicate		10.0	6.5
sulfate		200.0	88.7
chloridion		100.0	1486.0
bicarbonate		5.0	28.2
calcium		0	173.0
magnesium		0	9.5
aluminium		0	1.1

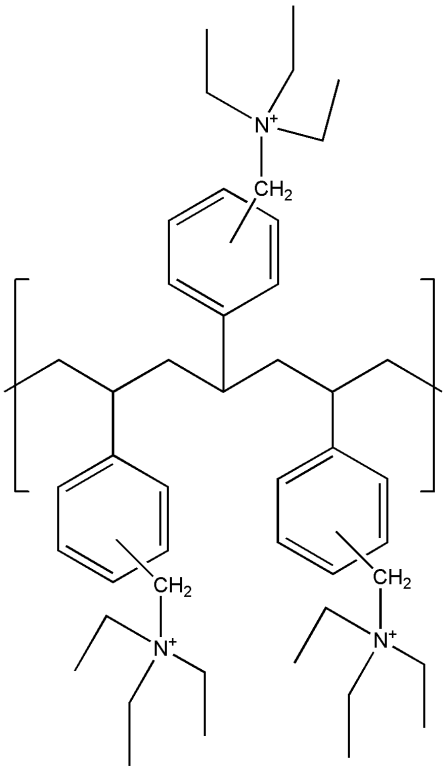

Fig. S1 Schematic illustration of the chemical structure of N201.

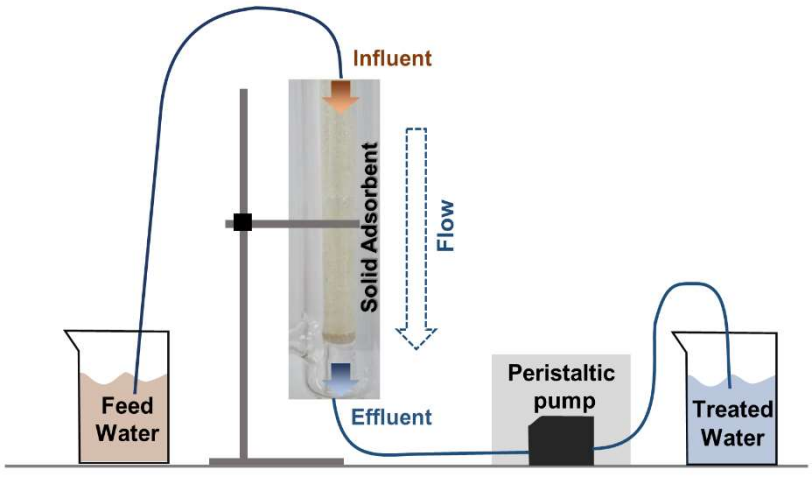

Fig. S2 Schematic illustration of the fixed-bed adsorption.

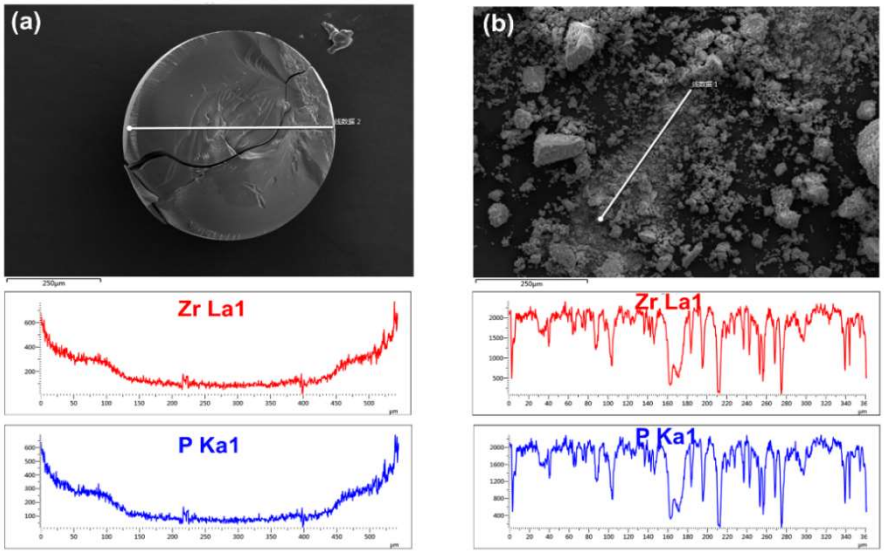

Fig. S3 The SEM and radial distribution of Zr and P elements in the (a) ZrP@N201 and (b) the bare ZrP.

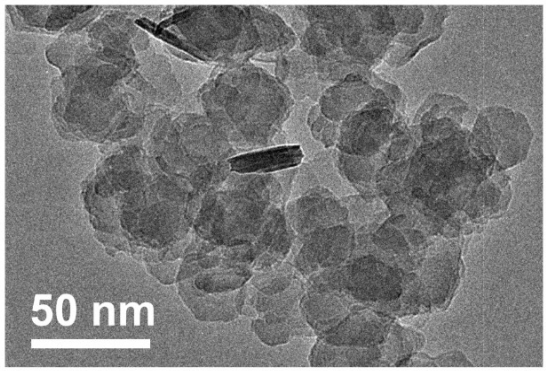

Fig. S4 TEM image of the bare ZrP.

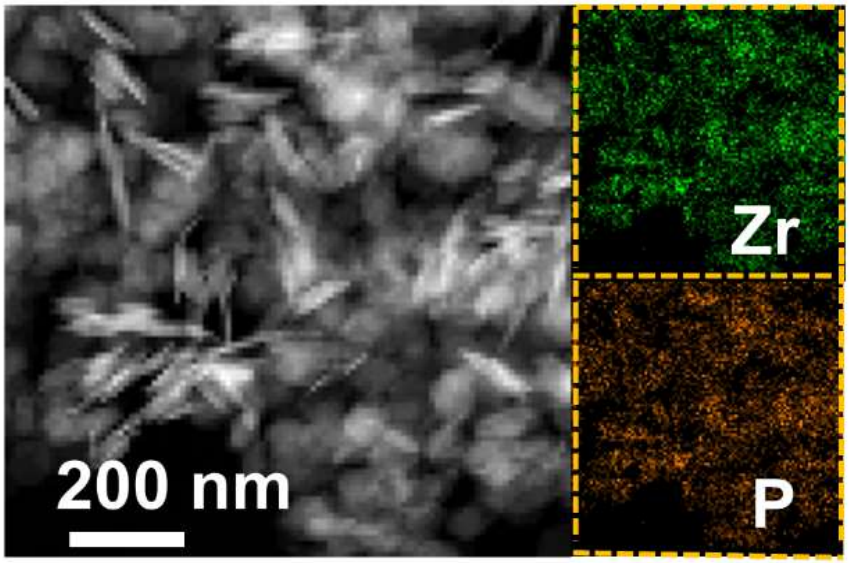

Fig. S5 HADDF-STEM and corresponding EDS elemental mapping of Zr and P of the bare ZrP.

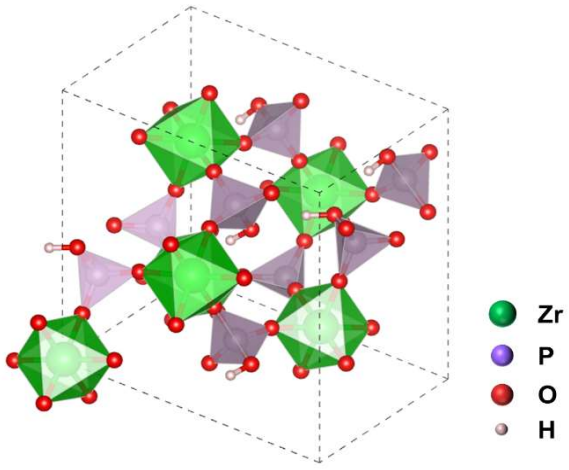

Fig. S6 Illustration of α-ZrP structure.

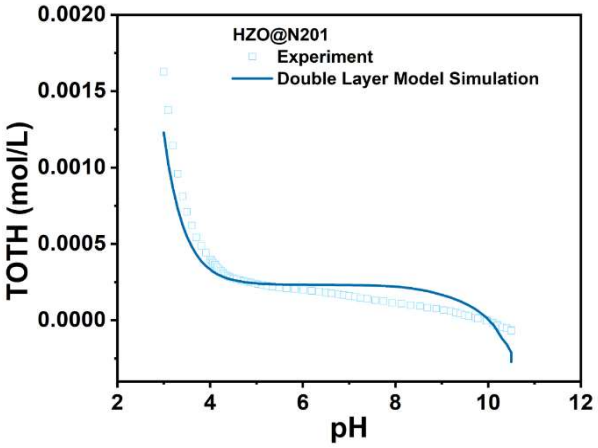

Fig. S7 Potentiometric titration of HZO@N201 fitting with double layer model.

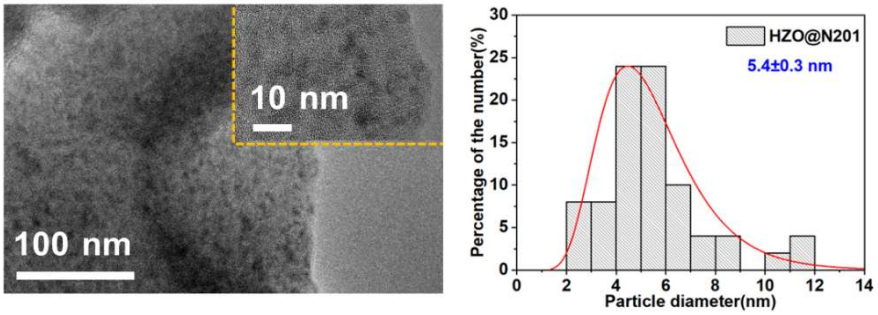

Fig. S8 TEM image of HZO@N201 and nanoparticles size distribution.

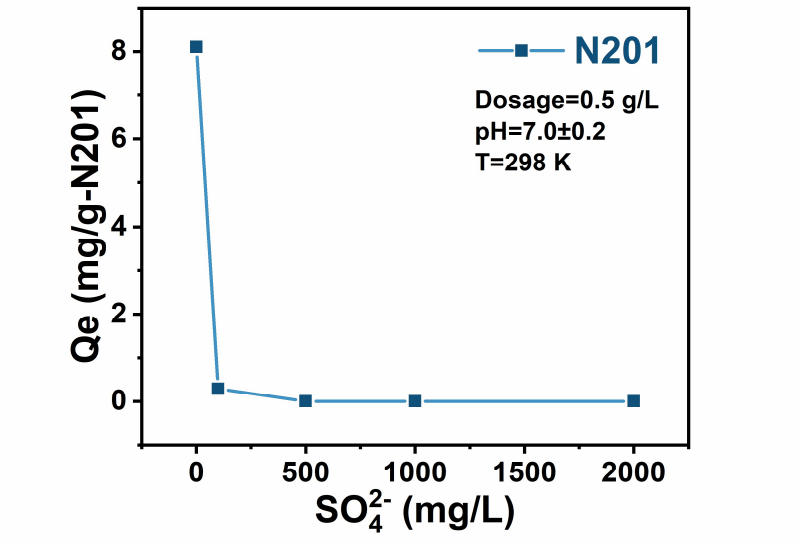

Fig. S9 Effect of sulfate on fluoride removal by N201 host (Solid dosage = 0.50 g/L, $[F^-]_0$ = 10 mg/L, pH = 7.0, t = 298K).

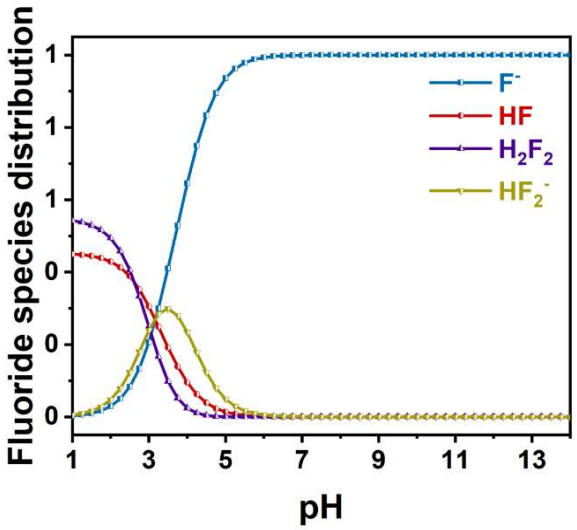

Fig. S10 Species distribution of fluoride ion in aqueous solution as functions of pH (calculated by Visual Minteq ver 3.0).

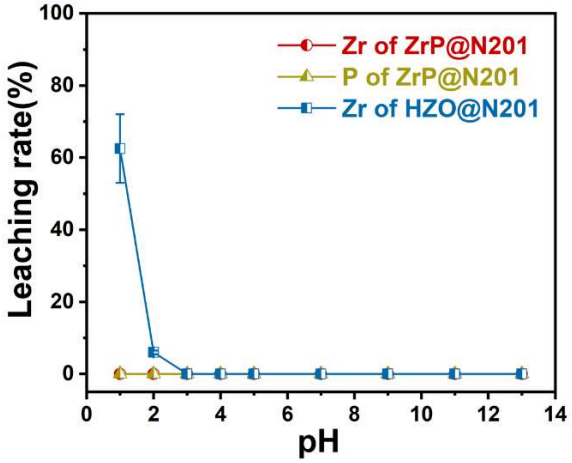

Fig. S11 Stability of ZrP@N201 and HZO@N201 under strong acids and bases solutions.

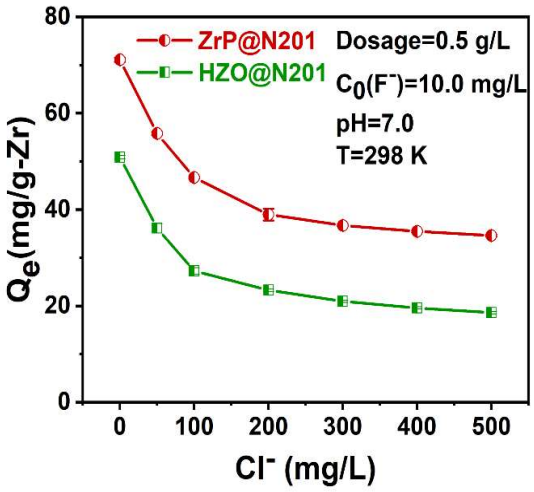

Fig. S12 Effects of chloride on adsorption capacity of HZO@N201 and ZrP@N201 toward fluoride.

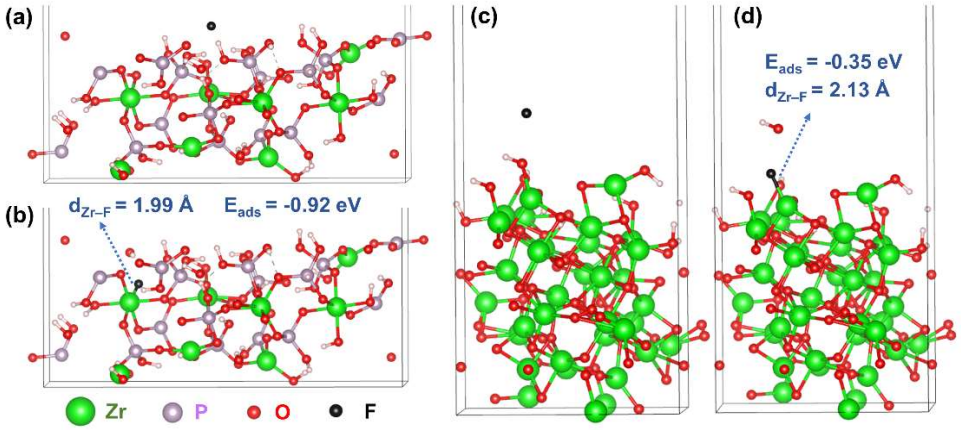

Fig. S13 Optimized (a, b) amorphous ZrP plane and (c, d) amorphous HZO plane slab models before and after fluoride uptake.

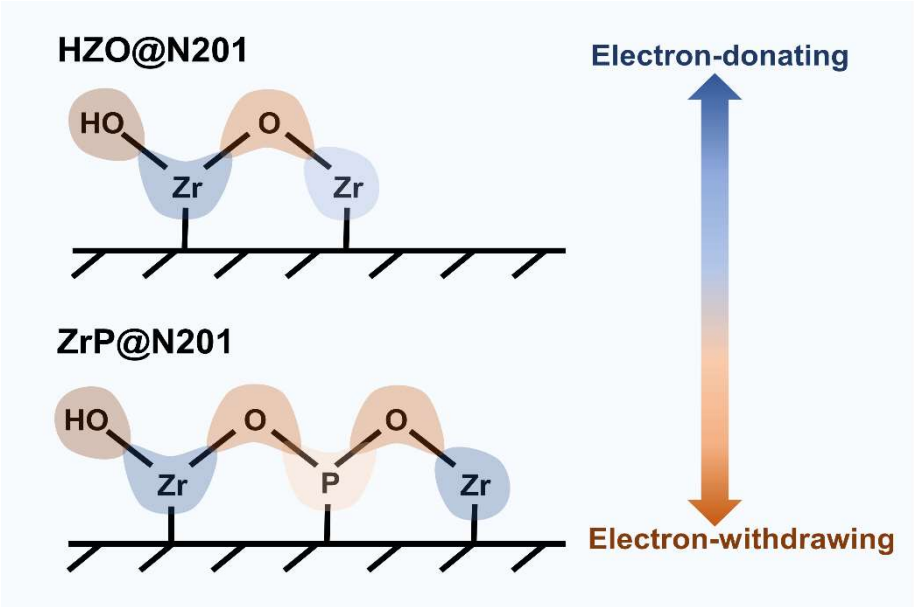

Fig. S14 Schematic illustration of the surface of HZO@N201 and ZrP@N201.

References

Ataka K i, Yotsuyanagi T, Osawa M (1996). Potential-dependent reorientation of water molecules at an electrode/electrolyte interface studied by surface-enhanced infrared absorption spectroscopy. Journal of Physical Chemistry, 100(25): 10664–10672

Kresse G, Joubert D (1999). From ultrasoft pseudopotentials to the projector augmented-wave method. Physical Review B: Condensed Matter, 59(3): 1758–1775

Lützenkirchen J (1998). Comparison of 1-pk and 2-pk versions of surface complexation theory by the goodness of fit in describing surface charge data of (hydr)oxides. Environmental Science & Technology, 32(20): 3149–3154

Martínez L, Andrade R, Birgin E G, Martínez J M (2009). Packmol: A package for building initial configurations for molecular dynamics simulations. Journal of Computational Chemistry, 30(13): 2157–2164

O'Connor N J, Jonayat A S M, Janik M J, Senftle T P (2018). Interaction trends between single metal atoms and oxide supports identified with density functional theory and statistical learning. Nature Catalysis, 1(7): 531–539

Perdew J P, Burke K, Ernzerhof M (1996). Generalized gradient approximation made simple. Physical Review Letters, 77(18): 3865–3868